Polymer-Derived Ceramic Coatings with Excellent Thermal Cycling Stability

Jan Bernauer,* Samuel Aeneas Kredel,* Emanuel Ionescu, and Ralf Riedel*

In the present work, transition metal-containing preceramic silicon polymers were synthesized via chemical modification of a commercially available organopolysilazane with Hf and Ta amido complexes as well as with borane dimethyl sulfide complex. The incorporation of transition metals into the polymer structure, their influence on ceramization and processability were thoroughly investigated. Moreover, the prepared preceramics were coated onto silicon wafers via spin coating and converted into crack-free, amorphous SiHfTa(B)CN-based ceramic coatings with excellent adhesion to the substrate. The composition of the ceramic coatings was investigated via X-ray photoelectron spectroscopy (XPS) and their high-temperature behavior was studied via oxidation tests performed at 1100 °C. Moreover, a thermal cycling procedure to temperatures above 1250 °C with rapid heating and cooling rates (i.e., in the range of 100–120 K s^{-1}) was applied to the ceramic coating, which showed no damage even after ten thermal cycles, indicating their outstanding performance and their potential for use as environmental barrier coatings at high temperatures.

1. Introduction

Thermal barrier coatings (TBCs) and environmental barrier coatings (EBCs) have gained significant interest in recent years due to their potential to protect high-temperature components, such as those found in gas turbines or in advanced propulsion systems.[1,2] TBCs mainly increase the maximal operation temperature of the material system by providing appropriate thermal insulation, while EBCs protect materials from degradation due to corrosive species present in the environment. Hence, the materials used in TBCs should possess low thermal conductivity and

J. Bernauer, S. A. Kredel, E. Ionescu, R. Riedel
TU Darmstadt
Institute for Materials Science
Otto-Berndt-Str. 3, 64287 Darmstadt, Germany
E-mail: jan.bernauer@tu-darmstadt.de;
samuel_aeneas.kredel@tu-darmstadt.de; ralf.riedel@tu-darmstadt.de

E. Ionescu
Fraunhofer- Einrichtung für Wertstoffkreisläufe und Ressourcenstrategien IWKS
Fraunhofer IWKS
Brentanostr. 2a, Alzenau 63755, Germany

possibly high thickness, whereas those used for EBC purposes should be dense, crack-free, and provide an effective diffusion barrier for corrosive species. In addition, materials used for both EBCs and TBCs require high phase stability, wear resistance, chemical compatibility as well as a low mismatch in coefficients of thermal expansion (CTEs) with the substrate and good adhesion to grant resistance to intensive thermal cycling, as this is a major cause of coating failure.[2,3] Next to the commonly utilized yttria stabilized zirconia (YSZ) which demonstrates a low thermal conductivity and a well-matching thermal expansion to the commonly used nickel-based superalloys,[4] ultra high-temperature ceramics (UHTCs) have been of great interest for high-temperature applications, which go beyond that of YSZ.[5] This group of ceramics with melting points above 3000 °C includes borides, carbides, and nitrides of the group IV and V transition metals.[6] In addition to the excellent thermal properties, these ceramics display chemical inertness and high hardness, caused mainly by the strong covalent bonding nature of the compounds but often suffer from a conditional oxidation resistance under high-temperature and oxygen-containing atmospheres.[7,8] Furthermore, their complex processing limits their use in many applications.[9]

The polymer-derived-ceramics (PDC) route offers a promising alternative for processing of UHTCs at lower temperatures and pressures, and particularly composites with high content of silica former (≈80 vol%) are accessible.[10] This general strategy involves transforming preceramic polymers into ceramic material by pyrolysis. In the case of UHTC-composites, transition metal compounds are used to modify the silica-former polymeric precursors and tailor the chemical composition and structure. As a result, the preceramic polymers can be designed in a way to match the desired properties required for any kind of barrier coating. Previous studies have shown the successful synthesis of liquid polymeric precursors for SiHfBCN- and SiZrBCN-based ceramics by modifying the commercial polysilazane Durazane 1800. The chemical structure of the precursors, as well as the high-temperature evolution of the resulting ceramics, was investigated in detail.[11,12] Further, sintered bulk samples of SiHfBCN showed promising results in short-term oxidation tests and spin-coated SiHfBCN samples demonstrated effective coatings with favorable oxidation behavior on chromium substrates.[13] Latest publications show that incorporating Ta to HfC/SiC monoliths leads to the formation of (Hf,Ta)C solid

solutions in SiC, improving the oxidation resistance of the nano-composites.[14,15] Therefore, the synthesis procedure of liquid Si(M)CN or Si(M)BCN precursors by modifying Durazane 1800 seems to be a promising approach to obtain materials for environmental or thermal barrier coatings. Remaining challenges for high-temperature stable PDC coatings are ensuring similar CTEs (coefficients of thermal expansion) between the substrate and the coating as well as good substrate adhesion.[16]

Additionally, the PDC route offers the possibility to obtain amorphous ceramics, thereby eliminating grain boundaries which can make ceramics prone to cracking under thermal shock conditions when grain boundary fracture energy is not sufficiently high.[17] A typical weakness of ceramics in EBCs or TBCs are phase transformations during thermal cycling and thermal shock, either by changing crystal structure or by the crystallization of amorphous ceramics which can lead to cracking when approaching temperatures of 1000 °C.[18–20] PDCs can overcome this problem through excellent crystallization resistance known for several systems, such as SiOC, SiCN, and SiBCN.[21,22]

In this work, we modified the commercially available preceramic copolymer Durazane 1800 with the transition metals hafnium and tantalum in the ratio 7:3 and different boron ratios to obtain liquid single-source precursors (SSP) with the composition $Si_x(Hf_{0.7}Ta_{0.3})_w(B_{var})C_yN_z$. The liquid precursor with excellent solubility was structurally investigated and coated on silicon substrates. The presence of reactive groups allowed a crosslinking step and a high ceramic yield. After pyrolysis, a homogeneous and crack-free ceramic coating was obtained, showing good short-term oxidation behavior and excellent adhesion. The adhesion and thermal shock resistance of the coating was tested in our study by using a self-built furnace with extreme heating rates of $\approx 170\,K\,s^{-1}$. The rates can be achieved by resistively heating 2 carbon strips directly in contact with the bottom and top of a flat sample. Due to their low thermal mass, they also cool down extremely fast with cooling rates of $\approx 140\,K\,s^{-1}$ down to 700 °C allowing very short cycle times (in this study, ten cycles within 10 min). Further, the thermal shock test is performed in inert atmosphere. Hereby, this method is able to focus on the thermally induced tensions, effectively emulating thermal shock in the system, strongly reducing simultaneously occurring processes such as oxidation or grain growth when compared to thermal shock tests performed for longer times or in air.

2. Experimental Section

2.1. Synthesis of Hf/Ta/B Modified Organopolysilazanes

The different SSPs were synthesized by modifying a commercially available organopolysilazane, namely Durazane 1800 (Merck KGaA) with tetrakis(diethylamino)hafnium (TDEAH, 99.99% trace metal bases, Sigma-Aldrich) and pentakis(dimethylamino)tantalum (PDMAT, 99.99% trace metal basis, Sigma-Aldrich). The molecular structure of the compounds used is depicted in **Figure 1**.

The weight ratio of Durazane 1800: (TDEAH + PDMAT) was set to approximately 65:35, a composition that has shown promise in obtaining soluble precursors,[8,9] while the molar ratio of the two transition metals, Hf:Ta, was set to 7:3. For
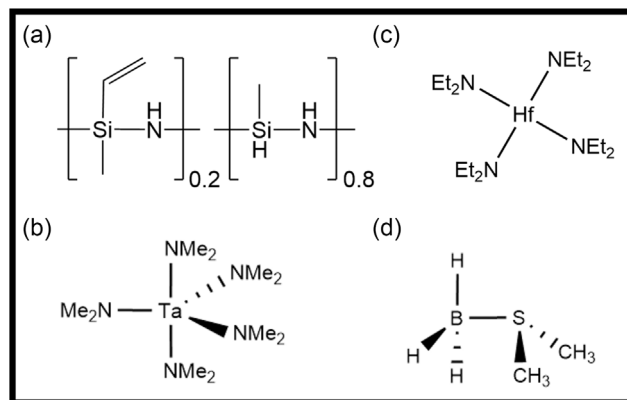

Figure 1. Chemical compounds used during the synthesis procedure. a) Durazane 1800, b) pentakis(dimethylamino)tantalum, c) tetrakis (diethylamino)hafnium, and d) borane dimethyl sulfide complex.

simplification, the composition $Si_x(Hf_{0.7}Ta_{0.3})_wC_yN_z$ is named B00 to distinguish between the samples with the boron-containing ones. For the $Si_x(Hf_{0.7}Ta_{0.3})_w(B_{var})C_yN_z$ samples, additionally, borane dimethyl sulfide complex (BMS, Sigma-Aldrich) was added, setting a transition metal:borane molar ratio of 1:0.5 (B05) and 1:1 (B10). For example, the synthesis of the single-source precursor (SSP) B10 was performed under an argon atmosphere using the Schlenk technique and glovebox. Typically, in a 250 mL Schlenk flask, 10.8 g of Durazane 1800 was dissolved in 20 mL of anhydrous toluene. To this solution, 4.20 g TDEAH and 1.55 g PDMAT, dissolved in 15 mL of toluene, were added dropwise. The newly obtained solution was stirred for 2 h at room temperature. Later, the solution was cooled by a mixture of dry ice and isopropanol to −78 °C and a solution of 0.96 g of BMS in 12 mL of toluene was added. The solution was allowed to reach room temperature and stirred overnight. The solvent was then removed under vacuum at 50 °C. The obtained SSPs are yellow- to brown-colored highly viscous liquids.

2.2. Spin Coating

The overall processing route from the commercial precursor to the ceramic coatings is displayed in the flow chart in **Figure 2**. After synthesis, three solvent-free SSPs with varying boron content were dissolved in anhydrous toluene (99.8%, Sigma) at a concentration of 35 wt% to prevent further crosslinking. In addition, diluted solutions with a concentration of 30, 20, and 14 wt% were prepared from the concentrated solution. Due to its tendency to hydrolyze, the non-crosslinked polymer was strictly manipulated under argon atmosphere. The substrates, 1 inch single crystalline silicon wafers (Prime CZ-Si, 280 μm, 2-side polished, MicroChemicals), were cleaned by repeatedly spinning off toluene. To later measure the thickness of the coatings, part of the substrate was taped off. As a coating technique, static spin coating was chosen due to its previous success for similar systems and good reproducibility.[23–25] The substrate was wetted with the filtered polymer solution (0.2 μm mesh size, 25 mm hydrophobic PTFE syringe filter, ROTILABO), accelerated to the target frequency by a spin coater (KL-SCI-20 with a one-inch spinning table, Quantum Devices) and then stopped after 40 s.
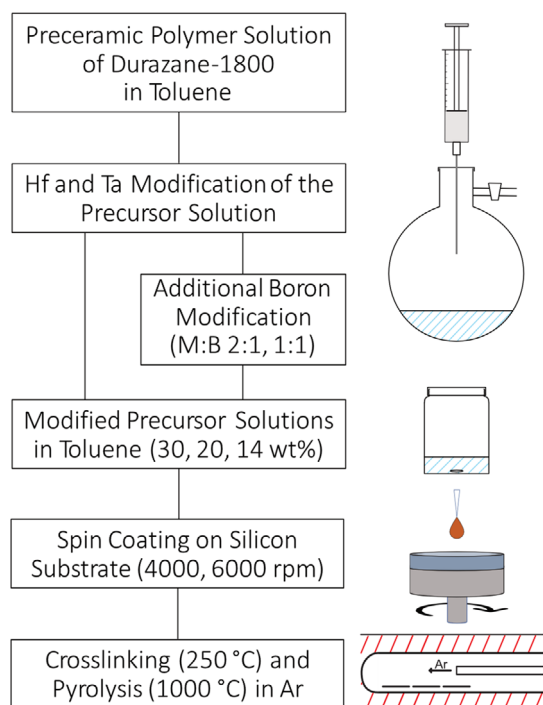
Figure 2. Flow diagram illustrating the preparation of ceramic coatings via spin-coating of the synthesized SSPs.

For those samples where an edge was taped off for subsequent profilometry, the tape was removed. After optimization of the spinning frequency, as this will provide the highest film thickness, with 1000 rpm steps, the lowest frequency yielding homogeneous coatings was chosen. The 14 wt% solutions were accelerated up to 4000 rpm for all boron contents, while all other concentrations were accelerated up to 6000 rpm. To crosslink the samples, they were placed into a quartz tube, which was then heated in a tube furnace (LOBA tube furnace) to 250 °C for 2 h with a heating and cooling rate of $100 \, \mathrm{K \, h^{-1}}$ under flowing Ar. Directly after performing profilometry, the samples were shortly washed with strong nitrogen gas flow to remove possible dust particles and put back into a quartz tube, which was then evacuated and flooded with argon three times, followed by a heat treatment at 1000 °C for 2 h with a heating and cooling rate of $100 \, \mathrm{K \, h^{-1}}$.

2.3. Characterization Methods

Fourier-transform infrared spectroscopy (FT-IR) in attenuated total reflectance (ATR) mode of the SSPs, the crosslinked powders and the ceramic films was carried out on a Varian 670-IR (Agilent, USA) in the range of $4000–550 \, \mathrm{cm^{-1}}$. Liquid-phase nuclear magnetic resonance (NMR) spectroscopy experiments of the SSP (^{11}B, ^{13}C, and ^{29}Si) were carried out on a Bruker AV 500 spectrometer (Bruker, Germany). For all NMR experiments, $CDCl_3$ was used as the solvent. Chemical Shifts are referred to TMS (tetramethylsilane) as the standard for ^{13}C and ^{29}Si NMR spectroscopy and to $BF_3 \cdot Et_2O$ for ^{11}B NMR studies. Rheological experiments were performed with a HAAKE
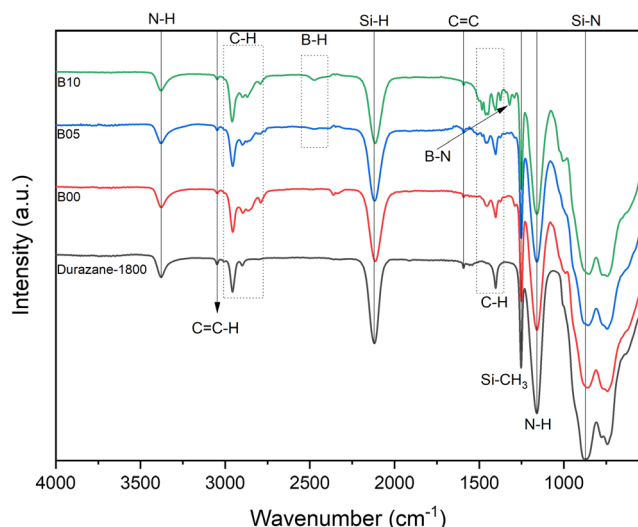
MARS I Rheometer (Thermo Fisher Scientific, USA) at room temperature. The ceramization process from the polymeric precursor to the ceramic product was investigated on powder samples. Therefore, the single-source precursor was crosslinked at 250 °C in argon to obtain a less air-sensitive powder. The thermal gravimetric analysis was performed at a STA449C Jupiter (Netzsch, Germany) with a heating rate of $5 \, °C \, min^{-1}$ from room temperature to 1100 °C in argon atmosphere. MAS NMR experiments were carried out on a Bruker Avance II+ spectrometer at 400 MHz proton resonance frequency, employing a Bruker 4 mm double resonance MAS probe at spinning rates of 12 kHz at room temperature. Single pulse (SP) ^{29}Si NMR spectra were recorded using a 90° pulse of 9 µs and recycle delays of 120 s. For the SP ^{13}C NMR spectra, a 90° pulse of 4 µs and recycle delays of 20 s were adopted. For the rheological measurement, we removed the solvent under vacuum at 50 °C, and after a short storage period, the samples were measured with a plate-plate (PP) geometry rheometer. The static measurement was carried out under a nitrogen atmosphere, and the time was set to 7 min to obtain a stable result. The coatings were studied by the following techniques: optical microscopy with a ring light (Zeiss Axio Zoom.V16, ZEISS, Germany), scanning electron microscopy (SEM) for surfaces (JEOL JSM-7600F, JEOL Ltd., Chiyoda, Tokyo, Japan), and cross sections (PHILIPS XL30 FEG, Philips Electronics, Amsterdam, Netherlands), profilometry for coating thickness (DektakXT, Bruker, USA) as well as X-ray diffraction (STADI MP, Mo K_α with Ge (111) monochromator, STOE, Germany), X-ray photoelectron spectroscopy (XPS, VG ESCALAB 250 with Al K-alpha 1486.68 eV, Thermo Fisher, USA), and FT-IR (see above) for structure and composition analysis.

Static contact angle measurement was performed using the sessile drop method on an OCA-20 goniometer (DataPhysics Instruments GmbH, Germany) with seven 3 µL water droplets per sample. An oxidation test was performed in air in a muffle furnace (VMK 1600, Linn High Therm, Germany). A self-built ultrafast furnace was used to test the resistance to rapid thermal cycling. The assembly is located in a vacuum chamber and can be operated under vacuum and in Ar gas. The specimen is placed between two carbon papers and heated by resistance heating. The current controls the temperature that is read by a pyrometer (KTRD 1485, MAURER, Germany) for temperatures between 700 and 3500 °C. Below 700 °C, the temperature is not measured.

3. Discussion and Results

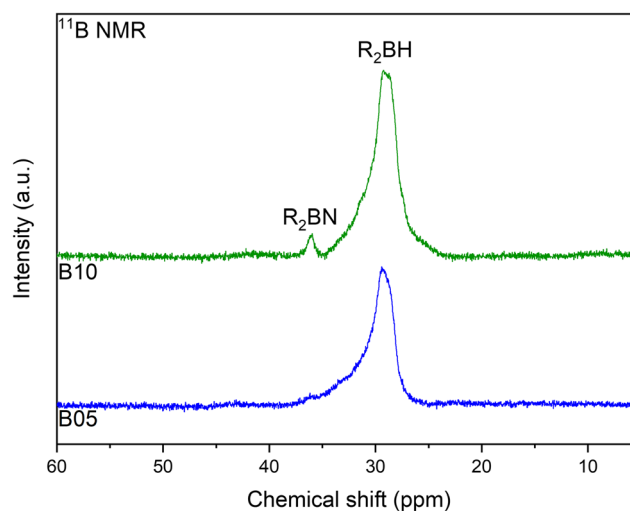### 3.1. Precursor Synthesis and Characterization

Complex multinary $Si_x(Hf_{0.7}Ta_{0.3})_w(B_{var})C_yN_z$ ceramics were synthesized from SSPs obtained via the reaction of the organopolysilazane Durazane 1800 with organometallic compounds of hafnium and tantalum and with a monoborane complex as described in the experimental section. The reaction was studied by FT-IR spectroscopy and ^{11}B, ^{13}C, and ^{29}Si liquid-phase NMR spectroscopy. The bare organopolysilazane is a copolymer comprised of vinyl/methyl silazane units (20%, A) and methyl/hydrido silazane units (80%, B). The FT-IR spectrum reveals structure-specific vibrations as displayed in **Figure 3**, namely N–H ($3389 \, cm^{-1}$), C–H ($2959 \, cm^{-1}$), Si–H ($2119 \, cm^{-1}$

ADVANCED
SCIENCE NEWS
www.advancedsciencenews.com

ADVANCED
ENGINEERING
MATERIALS
www.aem-journal.com

Figure 3. FT-IR spectra of Durazane 1800 and the modified polymers B00, B05, and B10 at RT.

Figure 4. ^{11}B spectra of the modified polymers B05 and B10 at RT.

(B)), C=C (1592 cm^{-1} (A)), Si–CH$_3$ (1252 cm^{-1}), Si–N–H (1165 cm^{-1}), Si–N–Si (889 cm^{-1}), and Si–C 751 cm^{-1}). The functional Si–H and N–H groups of the organopolysilazane undergo reactions with the organometallic compounds which lead to the formation of Si—N—M and N—M bonds (M = Hf, Ta) as has been reported in various previous studies.[11,26,27] Accordingly, an intensity decrease of the Si–H and the N–H vibrations is found in the FT–IR spectra of the metal-modified precursor. Despite the reduction of intensity, the vibration bands do not vanish entirely. Parallelly, for all systems, we find strong C-H vibrations at around 2800 and 1400 cm^{-1}. This result indicates that not all di(m)ethylamino ligands of Hf and Ta have reacted, most likely due to steric hindrances. The boron-modification of the SSP leads to B–H vibrations at 2485 cm^{-1} increasing with higher borane concentrations as indicated by the FT-IR spectra of the samples B05 and B10 in Figure 3. Besides the residual B–H vibrations after the hydroboration reaction between the vinyl groups of Durazane 1800 and the borane complex BMS, B–N vibrations (1324 cm^{-1}) are analyzed for sample B10. They can be ascribed to reactions of BMS with the polymer N–H groups or with the di(m)ethylamido ligands.

Besides IR spectroscopy, ^{11}B, ^{13}C, and ^{29}Si liquid-phase NMR experiments were conducted to investigate the underlying reaction mechanisms in more detail. ^{11}B spectra were measured for the boron-containing samples. The pronounced signal at $\delta = 29$ ppm in samples B05 and B10 is correlated to the hydroboration product R$_2$BH (R being an organic substituent) via the reaction of the BH$_3$ complex and the vinyl groups of the used organopolysilazane.[18] The broadened shape of the NMR peak indicates that both, namely α-addition (Markovnikov) and the β-addition (anti-Markovnikov), occur during hydroboration. The non-regioselective course of the reaction has already been described several times in the literature for similar experiments.[11,28] Additionally, for sample B10, a signal at $\delta = 36$ ppm originates from the discussed second reaction between N–H/R and B–H. Furthermore, none of the investigated samples displayed a signal of the starting BMS centered at

$\delta = -20$ ppm.[29] The corresponding NMR spectra are displayed in **Figure 4**.

The ^{13}C spectrum of Durazane 1800 in **Figure 5** exhibits four complex multiplett signals. Two of the signals correspond to the CH$_3$ groups bonded to silicon at $\delta = -1$ and $\delta = 5$ ppm while the peaks at $\delta = 130$ and $\delta = 140$ ppm are due to the C-atoms of the vinyl groups. The ^{13}C-NMR spectra of the metal and boron-modified samples become more intricate, revealing a new multiplett at $\delta = 36$–39 ppm, along with several singlet peaks distributed between $\delta = 40$–60 and $\delta = 15$–20 ppm. The complexity of the modified polymer hinders a straightforward assignment of the new signals to individual groups, as overlapping occurs due to similar chemical environments. The signals between 40 and 60 ppm can be assigned to N–CH$_n$ groups, leading to the conclusion that only a part of the organic N–(CH$_2$)–CH$_3$ groups react with the polymer backbone, with steric factors preventing further reaction. The signals in the range below 40 ppm are assigned to
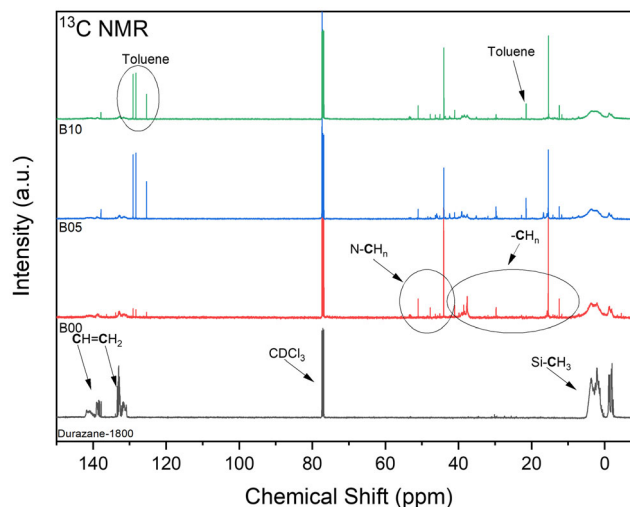
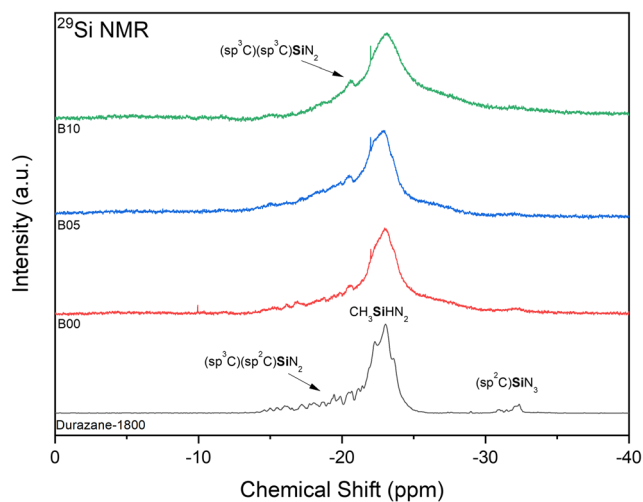**Figure 5.** ^{13}C spectra of Durazane 1800 and the metal-modified polymers B00, B05, and B10 at RT.

CH_n signals arising either from the transition metal compound or from carbon atoms of the hydroborated vinyl groups.[30–32]. Like the modified samples, the boron-free sample even shows a weakening of the vinyl signal. This aspect indicates a metal-induced catalytic hydrosilylation or vinylpolymerisation, specifically by the tantalum compound. Similar phenomena have already been observed for other vinyl-containing Si-polymers.[30]

In the ^{29}Si spectra of Durazane 1800 shown in **Figure 6**, a broadened peak between $\delta = -14$ and -21 ppm which is correlated to $(sp^2C)(sp^3C)SiN_2$ units occurs. A more distinct peak at -23 ppm is connected to CH_3SiHN_2 sites.[33] Additionally, smaller peaks are present at -32 ppm, which originate from $(sp^3C)SiN_3$ units caused by crosslinking of the organopolysilazane. The spectra of the modified organopolysilazanes look similar to that of Durazane 1800 and only the signal at -20.6 ppm became more pronounced, related to the formation of more C_2SiN_2 units caused by the reaction of the metal amido compound with the organopolysilazane. Further, the peak at

-23 ppm is broadened. The broadening is caused by increased polymer mass and the resulting restricted mobility of the polymer.[34,35] Based on the spectroscopic data, we propose the two reaction pathways for the synthesis of the single-source precursor of $Si_x(Hf_{0.7}Ta_{0.3})_w(B_{var})C_yN_z$ displayed in **Figure 7**. Accordingly, the organometallic compounds undergo reactions with Si–H and N–H groups of the organopolysilazane. The monoborane complex BMS undergoes a hydroboration reaction with the vinyl groups of Durazane 1800, which can lead to the respective Markovnikov and anti-Markovnikov hydroboration product.

The unmodified organopolysilazane is a low viscous liquid with a viscosity of 10–40 mPas. The modification with the organometallic compounds raises the viscosity drastically but, importantly, does retain good solubility in common aprotic solvents (THF, Toluene, Benzene, and Hexane). The static viscosity, shear storage moduli, and shear loss moduli were analyzed for the modified samples. The corresponding plots are displayed in **Figure 8** and the measured static viscosity, shear storage moduli, and shear loss moduli are listed in **Table 1**.

In the graph for the viscosities in Figure 8, we added the value for pure Durazane 1800 given by the technical datasheet. The modified polymers show a viscosity increase by six orders of magnitude which brings all samples in the range of 10^6 mPas. The samples B00–B10 do not differ much in the absolute viscosity, B00 shows the highest viscosity and B05 the lowest. However, the minor differences should not be overestimated, as they can also be attributed to minimal deviations in the synthesis or the drying process. More attention should be paid to the difference in the unmodified polymer. The extreme difference in viscosity is not noticeable after the reaction because the polymers are still diluted in toluene. In contrast, the polymer segments after vacuum drying are no longer surrounded by solvent molecules but rather by neighboring polymer chains and hence display greater interactions with each other. Furthermore, new polymer–polymer interactions caused by incorporating metals into the polymer backbone influence the conformation and, hence, thermophysical properties.[36,37] The presence of transition metal atoms can lead to ligand–metal donor–acceptor interactions with


Figure 6. ^{29}Si spectra of Durazane 1800 and the modified polymers B00, B05, and B10 at RT.
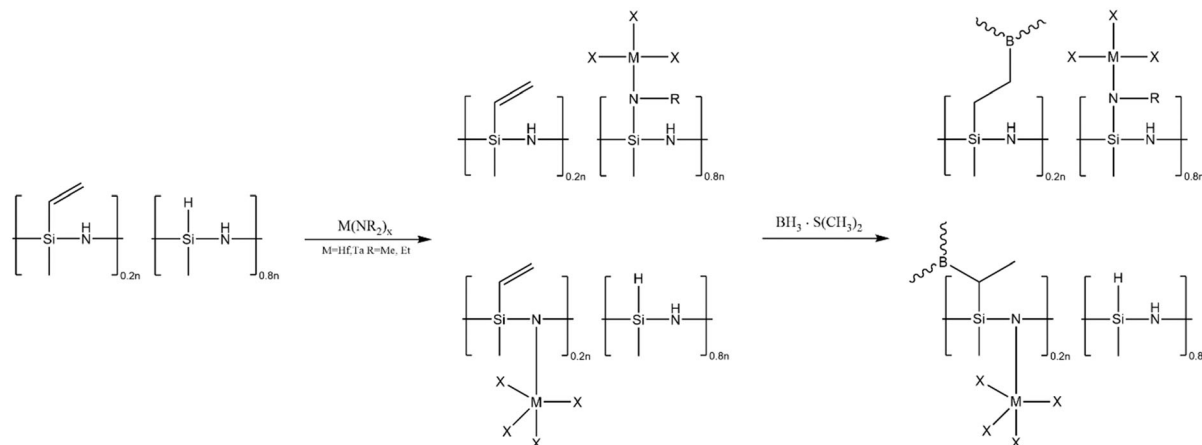
Figure 7. Proposed reaction pathways of synthesizing the SSP of $Si_x(Hf_{0.7}Ta_{0.3})_w(B_{var})C_yN_z$. The organometallic compounds undergo reactions with Si-H and N-H groups. BMS undergoes a hydroboration reaction with the vinyl group, which can lead to the Markovnikov and the anti-Markovnikov product.
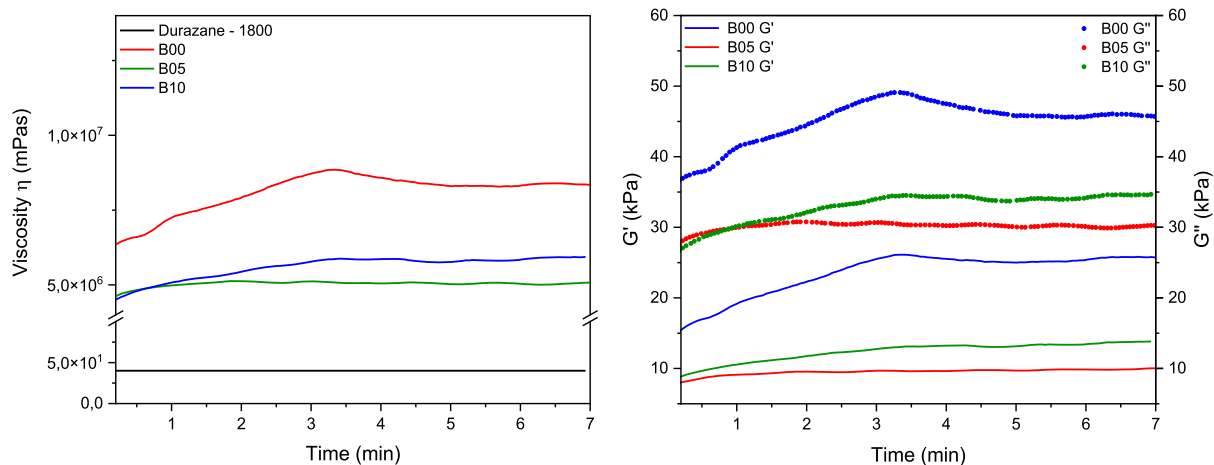
Figure 8. Static viscosity of Durazane 1800, B00, B05, and B10. Furthermore, the Shear storage moduli and Shear loss moduli of B00, B05, and B10 are depicted.

Table 1. Static viscosity, shear storage moduli, and shear loss moduli of Durazane 1800, B00, B05, and B10.
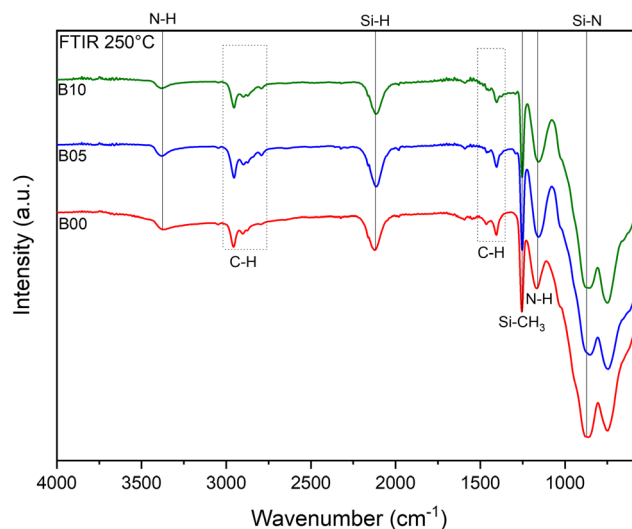
Sample	Viscosity [mPas]	Shear storage moduli [kPa]	Shear loss moduli [kPa]
Durazane 1800	10–40[a]	–	–
B00	8.4×10^6	25.6	45.8
B05	5.1×10^6	11.3	31.5
B10	5.8×10^6	13.6	34.4

[a]Durazane 1800 product data sheet.

Figure 9. FT-IR spectra of B00, B05, and B10 after crosslinking at 250 °C.

high coordination numbers in addition to the chemical bonds between polymer and metal. These supramolecular interactions are known from the literature for transition metals and materials containing anionic or neutral donor ligands like nitrogen.[38] The combination of supramolecular interactions as well as the probably increased molecular mass caused by the modification of the polymers contributes to the increased viscosity. While highly viscous, all samples displayed a G'' about 20 kPa higher than G'. The significantly larger G'' than G' moduli correspond to a liquid rheological behavior with fluid mechanics.

3.2. Polymer-to-Ceramic Transformation

The liquid SSP were cross-linked at 250 °C to investigate the pre-ceramic intermediate state during the early ceramization steps. FT-IR was used for the analysis of the modified and crosslinked samples displayed in **Figure 9**. In addition, we investigated sample B05 by ^{13}C and ^{29}Si MAS NMR spectroscopy. These spectra are shown in **Figure 10**. Additionally, the thermal transformation of the SSPs into amorphous ceramics was investigated by TGA. The measurements were performed on crosslinked powders to eliminate the effect of the substrate and get the information on only the polymer-derived material. Thus, the obtained results are substrate independent.

All samples show similar FT-IR-spectra and similar changes compared to the liquid precursor. The signal intensities of the Si–H (2119 cm^{-1}) and the N–H (3389 cm^{-1}) stretching bands clearly decrease. Besides, the vibration bands of the C=C groups are mostly diminished. The reduction of these bands can be correlated to the different reactions occurring during the crosslinking process. Reactions that utilize the aforementioned functional groups and lead to solid crosslinking in the preceramic state are hydrosilylation, which was already discussed in the previous section, namely the transamination and different dehydrocoupling reactions between Si–H/N–H.[39] The simplified dehydrocoupling reactions are shown in Equation (1) and (2).

Transamination (1)
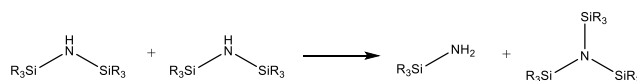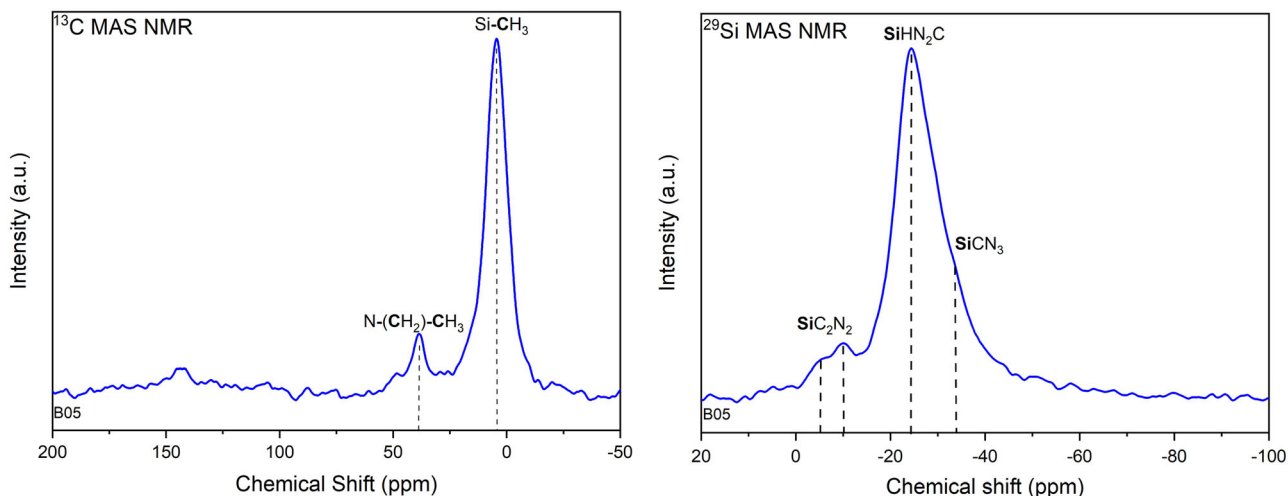
Figure 10. ^{13}C and ^{29}Si MAS NMR Spectra of the modified and crosslinked polymer B05 cured at 250 °C.

Dehydrocoupling (Si–H and N–H) (2)

The B–H/B–N bands are no longer visible in the FTIR spectra. This feature implies that the hydroboration and dehydrocoupling reactions with BMS are completed at 250 °C. Furthermore, the ethyl/methyl C–H vibrations band decreased in intensity. Combined with the reduction of the Si–H and the N–H stretching bands, it indicates an increased degree of crosslinking.[12]

The ^{29}Si MAS NMR of the cured sample B05 shows a broadened signal from −5 to −10 ppm caused by the presence of SiC_2N_2 units with sp^3 carbon with different chemical environments.[28] The broadening of the SiC_2N_2 sites is caused by the nature of the second coordination sphere, leading to a slightly higher or lower field shift depending on the substituents of C and N. The second observed signal appears at −17 to −40 ppm and can be traced back to overlapping signals of $SiHN_2C$, $SiCN_3$ with different coordination spheres.[28,40] ^{13}C MAS NMR spectra of the crosslinked polymer cured at 250 °C display a peak at −10 to 20 ppm. The broad signal is caused by the CH_3—Si bonds being situated in different copolymer parts, which was already observed in the precursor's liquid-phase NMR. Compared to the liquid NMR, the signal broadened because of the new environment sphere around the Si–CH_3 and the newly formed Si-CHR_2 groups.[34] Additionally, a peak at 39 ppm, assigned to N–(CH_2)–CH_3, is caused by the remaining homoleptic di(m)ethylamine ligands which were already found in the precursor.[41]

The thermal transformation of the SSPs into amorphous ceramics was studied by thermal gravimetric analysis (TGA). The corresponding TGA curves and their first derivatives (DTG) are shown in **Figure 11**. The three different samples display similar behavior during the ceramization process. The mass loss curves exhibit three plateaus leading to a ceramic yield of 81–82 wt%. The ceramization process for all samples is completed at 800–850 °C, as no mass loss can be found when heated
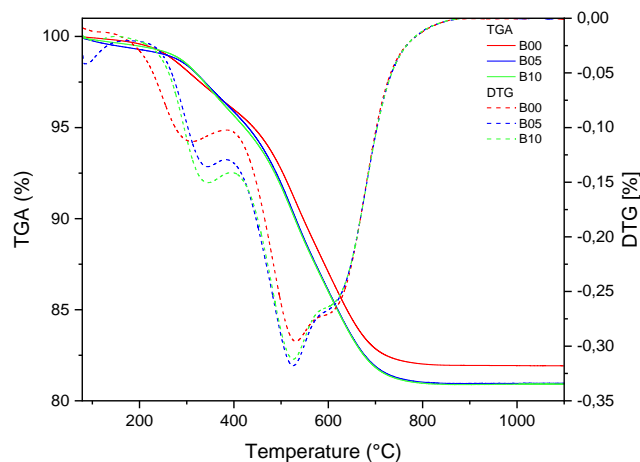
Figure 11. TGA and DTG of the modified polymer precursors.

to higher temperatures. Potentially, low amounts of hydrogen could still be released at higher temperatures, as this would only lead to minuscule weight loss. As this release of hydrogen might influence structure as well as density, the pyrolysis temperature for the coatings was set considerably higher, to 1000 °C.

The boron-free sample behaves slightly differently during ceramization compared to compounds containing boron which can be easily seen in the first sections of the DTG curves. The first minimum appears at 310 °C for B00 and is slightly offset from B05 and B10 (350 °C). The second major mass loss step occurs from ≈300 to 800 °C, wherein the boron-containing compounds lose more mass even if the progression is identical depending on the temperature. The total mass losses amount 18.1 wt% for B00 and 19.1 wt% for B05 and B10.

In previous studies, analogous mass yields were analyzed for $Si_x(Hf_{0.7}Ta_{0.3})_w(B_{var})C_yN_z$ and SiZr(B)CN polymer-derived ceramics. Pristine Durazane 1800, in contrast, displayed a mass yield of 65 wt%.[11,12,42] The strongly increased yield and, therefore, reduced volatilization during the ceramization process are

**ADVANCED
SCIENCE NEWS**

www.advancedsciencenews.com

**ADVANCED
ENGINEERING
MATERIALS**

www.aem-journal.com

beneficial for the intended application as it helps to prevent cracking of the coatings.[43]
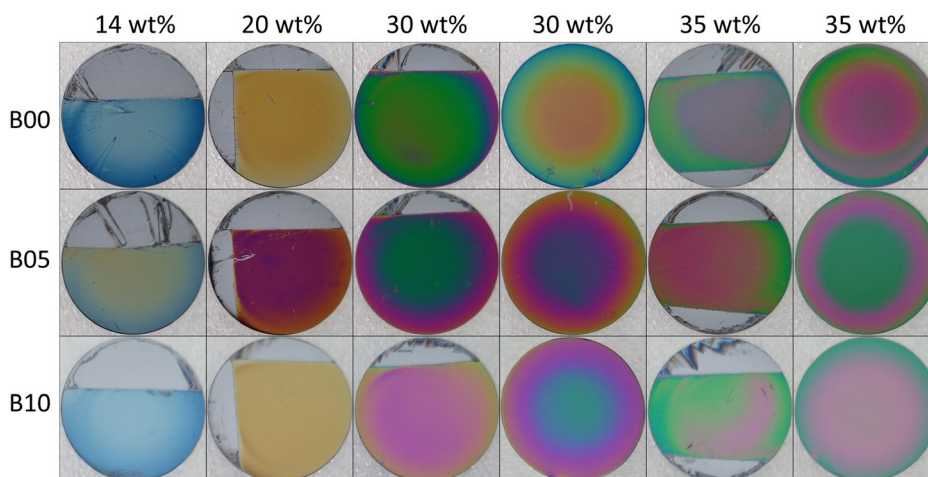
3.3. Coating

According to the results related to the precursor synthesis, characterization, and ceramization, our chemically modified preceramic polymers are suitable compounds to be applied for coating processes.[24] The SSPs are liquid, show good solubility in aprotic solvents and have reactive functional groups allowing crosslinking. In addition, less than 20% mass loss during polymer-to-ceramic transformation indicates the suitability of the PDC precursor for coating applications.[25]

In the following, the notation of the coated samples is composed of the solution concentration followed by the maximum temperature of thermal treatment and then the boron content of the polymer. For example, the crosslinked coating derived from the 35 wt% B10 polymer solution is denoted as 35wt250B10.

3.3.1. Coating Characterization

All coatings derived from freshly synthesized 14, 20, 30, and 35 wt% solutions are crack-free, as seen in **Figure 12**. While most of our sample coatings are primarily homogeneous, minor inhomogeneities accumulate near the taped-off region. They can be ascribed to particles being dissolved from the tape that was used to keep some part of the wafer uncoated to allow for thickness determination through profilometry. In addition, interference effects in layer thickness are found near the tape edge. More minor defects are seen throughout all samples, including those without taped-off edges. Most likely, they are caused by small particles contaminating the sample prior (radiating outwards from the defect, possibly also caused by gas bubbles) or after the coating process.

Aside from these defects, all coatings, especially those without taped-off edges, show good homogeneity. This is representatively shown in **Figure 13** for the 30 wt% samples by light microscopy images and in **Figure 14** by electron microscopy.
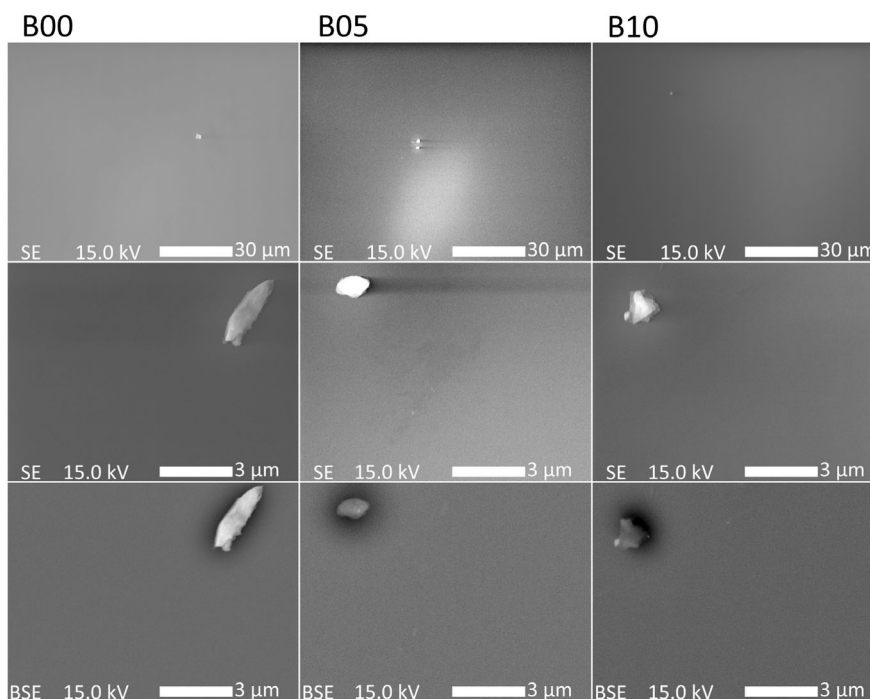

Figure 12. Images of top to bottom: 1000B00, 1000B05, 1000B10; left to right: 14 wt% 4000 rpm, 20 wt% 6000 rpm, 30 wt% 6000 rpm, 35 wt% 6000 rpm showing mostly homogeneous coatings for all concentrations and boron contents.
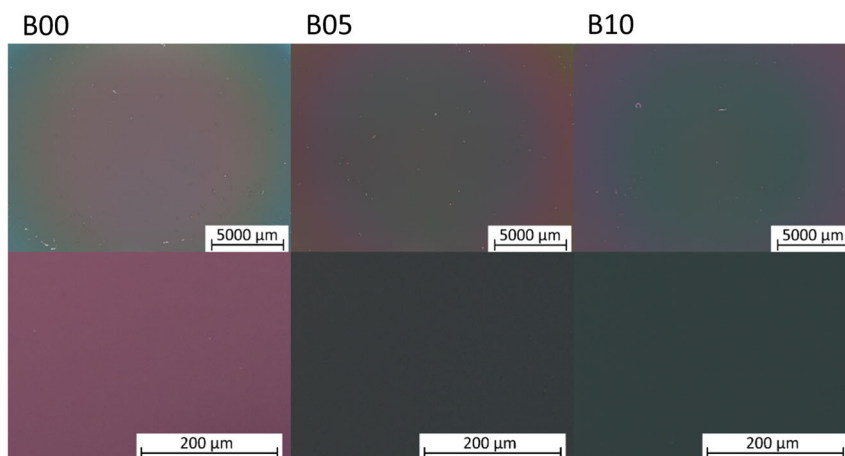
Figure 13. Microscopy images using a ring light. From left to right: 30wt1000B00, 30wt1000B05, 30wt1000B10.

Figure 14. SEM images of (left to right) 30wt1000B00, 30wt1000B05, and 30wt1000B10 at x1,000 magnification in SE mode (top), x10,000 magnification in SE mode (middle) and x10,000 magnification in BSE mode (bottom) with a dust particle to ensure the sample is in focus.

In SEM, both topography (SE images) and composition (BSE images) show good homogeneity with no apparent porosity, indicating high density and confirming the good processability of the preceramic polymers based on their aforementioned physical properties.[33]

The thickness of the crosslinked and pyrolyzed coatings, obtained from profilometry, is plotted over the concentration of the solution in **Figure 15**. The slight increase of the coating thickness from 14 to 20 wt% is caused by the frequency increase from 4000 to 6000 rpm.
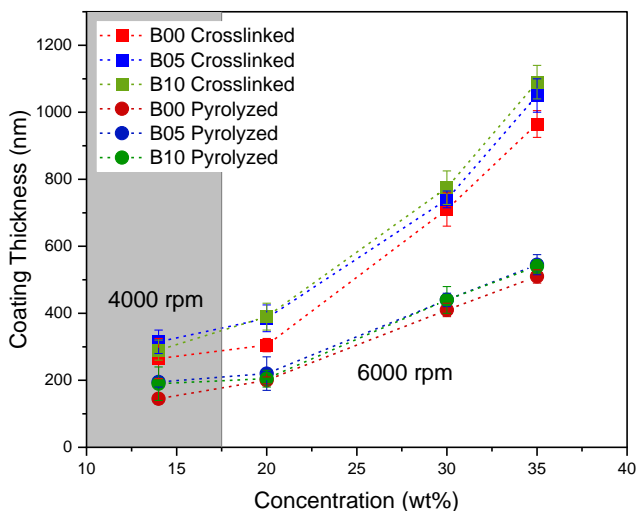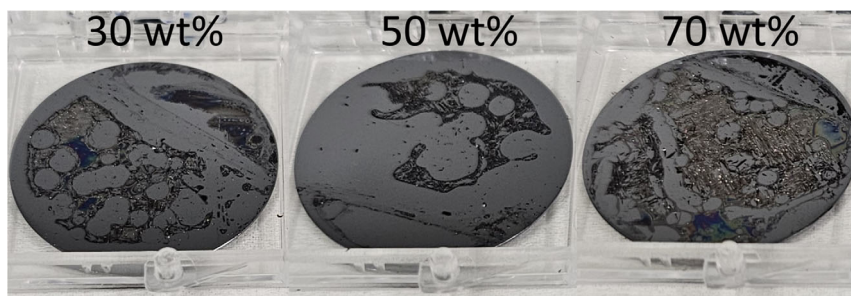

Figure 15. Coating thickness after crosslinking at 250 °C and pyrolysis at 1000 °C.

The thickness of the coatings ranges from ≈265 to 1090 nm after crosslinking and from ≈145 to 545 nm after pyrolysis. The shrinkage is constrained in two dimensions due to the adhesion to the substrate, meaning the volume shrinkage is directly represented through the thickness. The average volume shrinkage from crosslinked polymeric film to pyrolyzed ceramic film in this study is $43 \pm 4\%$.

To the best of our knowledge, there have been no publications on filler-free unmodified Durazane 1800 (or HTT 1800) derived ceramic coatings. In our tests however, all of its ceramic coatings strongly spalled off during thermal treatment at identical conditions, down to a thickness of roughly 270 nm for 30 wt% Durazane 1800 in toluene (see **Figure 16**).

We ascribe the significant improvement of the processability of the modified preceramic polymers to their strongly increased ceramic yield discussed in Section 3.2, most likely correlating to an increased crosslinking degree as well as increased molecular mass. They reduce the amount of evaporating light chains during pyrolysis and thus reduces the shrinkage from dry polymer film to ceramic. This reduces the stresses in the coating and the interface, hence increasing the critical thickness.

Overall, the coatings prepared from boron-modified polymers are about 14% thicker than that of the boron-free formulations, while no significant difference in thickness between the B05 and B10-derived coatings could be found. According to Meyerhofer's equations,[44] the film thickness is proportional to $\eta^{1/3}$. Considering that the measured viscosity of B00 is about 1.5 times that of the boron-modified samples, an increase in thickness for B00 samples above 10% would be expected.

ADVANCED
SCIENCE NEWS

www.advancedsciencenews.com

ADVANCED
ENGINEERING
MATERIALS

www.aem-journal.com

Figure 16. Coatings derived from pristine Durazane 1800 solutions of 30–70 wt% in toluene after crosslinking and pyrolysis. Thickness from ≈270 nm (30 wt%) to ≈540 nm (70 wt%) (determined by profilometry from spalled areas to remaining film).

As known for PDC coatings, they fail during thermal treatment when surpassing a critical coating thickness (t_c).[45] For the B05 precursor, this t_c was surpassed at 755 ± 30 nm after pyrolysis for a coating prepared from the 35 wt% B05 solution that had been aged for 2 weeks (evaporated toluene was accommodated for, images shown in Figure S1, Supporting Information).

To prolong the shelf life, the apparent crosslinking of the solvent, likely promoted by the introduced metals, Hf and Ta, which can catalyze hydrolysis or other polymerization reactions like hydrosilylation or hydroaminoalkylation,[30,46,47] should be counteracted. Hence, as a kinetic hindrance, the polymer precursor should be diluted and stored in a cooled opaque container – while ensuring an inert atmosphere. Nevertheless, the development of viscosity should still be monitored, or otherwise, test samples are required from time to time. To prevent the precursor aging via crosslinking, the polymer was immediately diluted to 35 wt% solution in toluene after drying. Furthermore, all coatings on which profilometry was performed and that are shown in Figure 12 were prepared on the day of drying the polymer, and additional samples for further investigations were prepared within 2 days after drying.

Further characterization of the structure and composition of the coatings was performed on the 30 wt% samples. All of them remained X-ray amorphous after pyrolysis at 1000 °C (see Figure S2, Supporting Information).

The elemental composition of the sample 30wt1000B05 measured by XPS and its theoretical composition are listed in **Table 2**. Since XPS is surface sensitive, the elemental composition is more precise after removing the naturally occurring thin carbon-rich layer by argon sputtering. However, this sputtering has a slightly reducing effect, so oxidation states of the species most likely not present in the carbon layer (Si, Hf, and Ta) were analyzed from the pristine XPS spectra.

The oxygen content of about 60 at% obtained from XPS means that at least the top 10 nm of the ≈440 nm thick coating were strongly oxidized, under the depletion of carbon and nitrogen, with the amounts for Si, Hf, and Ta being in good agreement with their theoretical concentration. This oxygen content is not high enough for complete oxidation both after sputtering (in which case the Ar$^+$ sputtering might have caused some oxygen depletion) and for the pristine sample, even under the assumption of carbon not being bonded to oxygen. For the sputtered sample, about 25% higher oxygen content would be required for the oxidic phases of SiO_2, HfO_2, and Ta_2O_5.
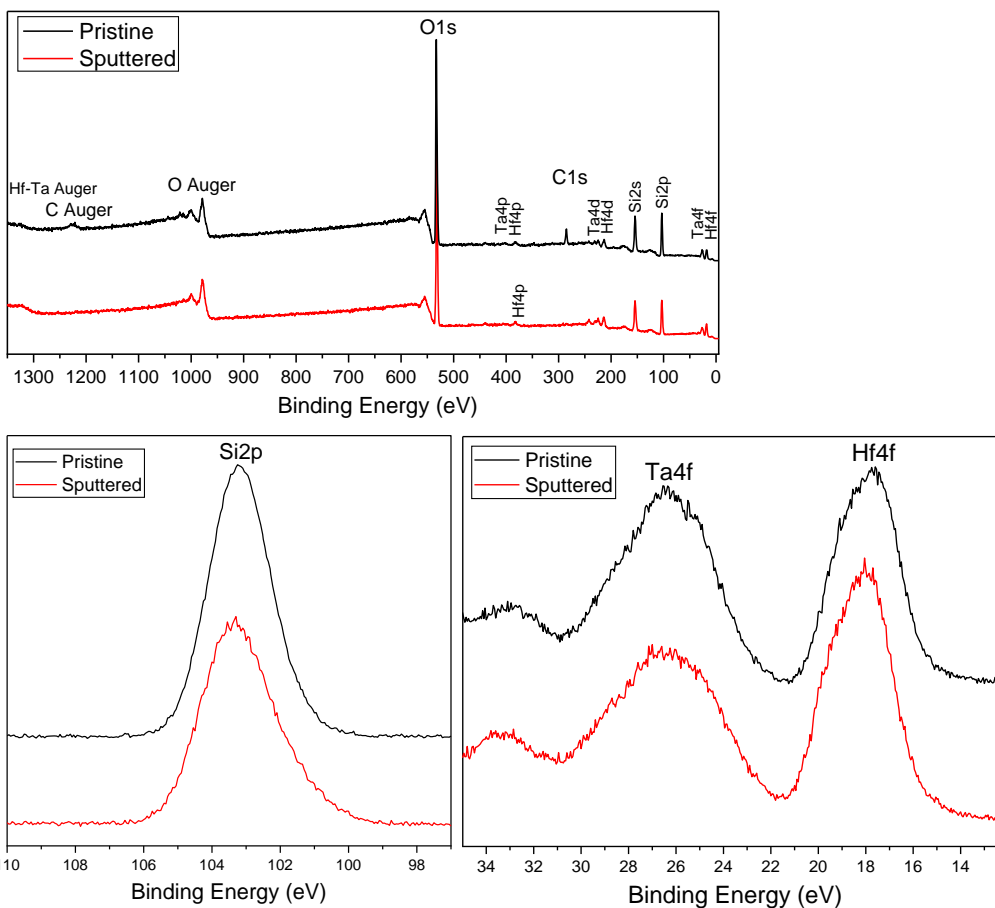
Both nitrogen and boron cannot be found in XPS, while the carbon content is significantly lower than that of the theoretical value. This is likely caused by oxygen replacing nitrogen and carbon under the formation of volatile carbon oxides, amines, and nitrogen oxides. Conversely, boron is likely not detectable due to its low theoretical content of about 1 at% in combination with its small cross-section.

In **Figure 17** the binding energies of silicon, hafnium and tantalum in the sample show an increase compared to the pure elements, situated in proximity but still below those of their oxides (103.5 eV for SiO_2, 18.3 eV for HfO_2, and 26.2 eV for Ta_2O_5). This means that while having bonds to oxygen, they also have bonds to other, less electronegative elements in the film. This supports the hypothesis that oxygen replaces bonds to nitrogen and carbon near the surface while leaving the polymer's metal(loid) backbone intact.
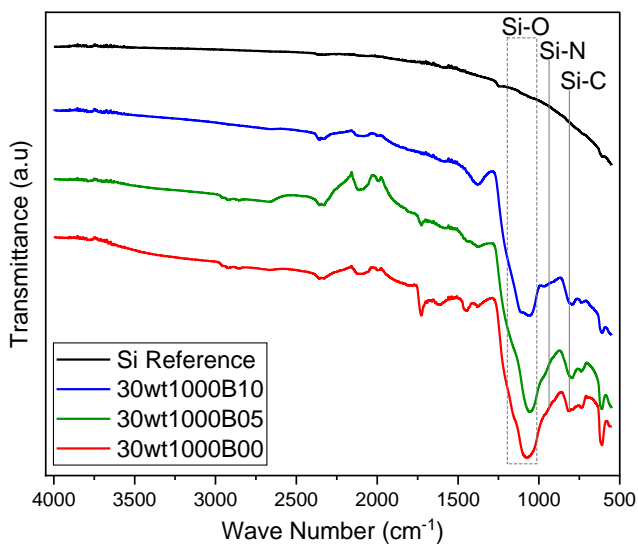
The oxidation is confirmed by the presence of Si–O band in FT-IR for all three ceramic coatings (see **Figure 18**). Since no oxidation of the precursor was found in FT-IR but can be seen for the pyrolyzed coatings, surface oxidation occurs during their thermal treatment or handling. This, most likely, is caused either by trace amounts of oxygen present in the argon atmosphere of

Table 2. Theoretical elemental composition (assuming full reaction of modifiers and full release of side groups and hydrogen), elemental composition extracted from XPS narrow spectra both pristine and after Ar$^+$ sputtering.

Concentration [at%]	Si	Hf	Ta	B	C	N	O
Theoretical	30.8	1.69	0.564	1.11	37.0	30.8	not expected
XPS pristine	31.7	1.06	1.01	not found	10	not found	55.6
XPS sputtered	34.5	1.65	1.07	not found	1.17	not found	60.1

**ADVANCED
SCIENCE NEWS**

www.advancedsciencenews.com

*ADVANCED
ENGINEERING
MATERIALS*

www.aem-journal.com

Figure 17. XPS overview spectrum and narrow spectra for Si2p, Hf4f, and Ta4f.

Figure 18. ATR Spectrum of 30 wt% coatings after pyrolysis showing strong Si–O bands.

the furnace, as previously reported for PDC coatings,[23,48] or the short handling of the samples in air after the crosslinking step for characterization.

As the film has a thickness of less than 0.5 μm and the oxidation takes place at the surface, the oxidation concerns a vastly increased portion of the sample volume when compared to powder or bulk samples, which is also the reason why they show a minuscule amount of oxygen compared to coatings. Due to this increased oxygen content in the coating observed in the nearly fully oxidized surface, the composition is strongly shifted from the expected $Si_x(Hf_{0.7}Ta_{0.3})_w(B_{var})C_yN_z$ towards $Si_x(Hf_{0.7}Ta_{0.3})(B_{var})O_a$.

The surface properties of the B05-derived coatings were also studied by water contact angle (WCA) measurements of the silicon wafer, the crosslinked coating and the pyrolyzed coating (see Figure S3, Supporting Information). The Si wafer is hydrophilic with a WCA of 53.8(8)°, correlating to a thin, naturally grown oxide layer on the wafer surface.[49]

The crosslinked polymeric coating decreases the surface energy, being only slightly hydrophilic with a WCA of 83.9(15)° which is lower than that of the WCA of 90–96° provided

by the manufacturer of the polymer (Merck, Germany). Instead of the polymer modification, the crosslinking temperature is most likely the dominant factor for this difference as reported in previous studies on the WCA of Durazane 1800 coatings, where the WCA was found to be 103° when crosslinked at room temperature, due to present Si-CH$_3$ and Si–CH=CH$_2$ groups that are not involved in crosslinking at that temperature and then continuously decrease with rising crosslinking temperature to 97° at 130 °C, 87° for 200 °C, and 78° for 300 °C.[24,31,50]

The found WCA in this study of 84° after crosslinking at 250 °C falls well into this dataset. This means that the less oxidizing atmosphere and the chemical modification are having a similarly significant effect on surface energy, negating each other, or both having only a minute impact. As Wang et al. found that Si—H bonds remain predominant in perhydropolysilazane even if crosslinked in air for temperatures below 300 °C, we expect both factors to have little impact.[51]

After pyrolysis, the coating is strongly hydrophilic, with a WCA of 37.7(18)°. This can be explained by the removal of the hydrophobic groups during pyrolysis as well as the surface oxidation shown by XPS. Hence, at the interface between wafer and coating, the WCA of the substrate and the coating are expected to be quite close and between 45°–60°, so good adhesion is anticipated.[52]

3.3.2. Adhesion, Oxidation, and Thermal Stress

Attempts to quantify the adhesion of the coating to the substrate were made. However, cross-cut tests could not be performed successfully because the force required to cut through the ceramic layer could not be supported by the silicon substrate, leading to brittle fracture. Still, in cross sections of the 30 wt% samples investigated by SEM, suitable adhesion between coating and substrate is shown by means of good contact between coating and substrate as shown for sample 30wt1000B05 in **Figure 19**. The excellent adhesion can be explained by the surface Si–OH groups of the silicon wafer reacting with the Si-H groups of the silazane precursor, forming Si—O—Si bonds.[53] Further, the cross-section again shows good homogeneity and evenness of the coating.

To test the suitability of the coating for possible application in high-temperature environment, a first oxidation test of a
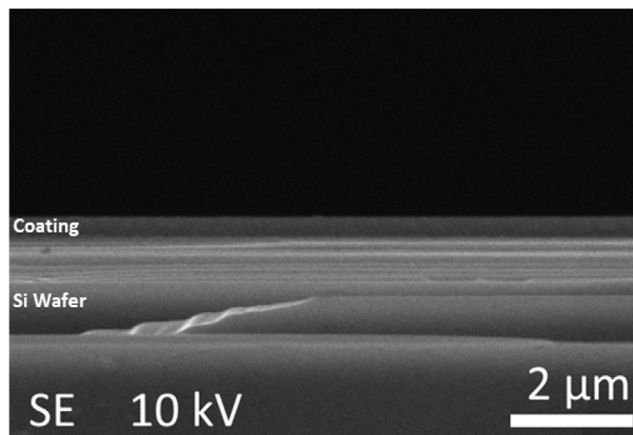
Figure 19. SEM image of the cross-section of sample 30wt1000B05.
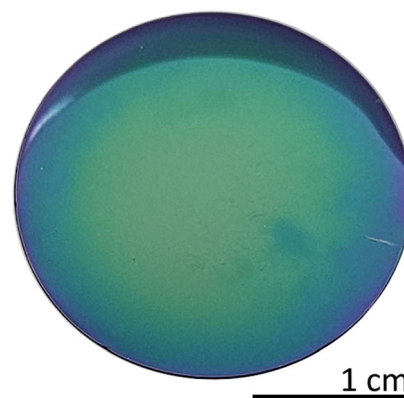
Figure 20. Image of 30wt1000B05 after 10 h of oxidation in air at 1100 °C.

30wt1000B05 sample was performed in air at 1100 °C for 10 h (heated to 1100 °C in 1 h and cooled below 600 °C within 1 h. After 10 h of oxidation, the coating shows no signs of failure, as can be seen in **Figure 20**.

During the lifetime of an environmental barrier coating, it is usually exposed to repeated temperature changes between room and operating temperature. In addition to thermal fatigue, poor thermal shock behavior can cause failure during rapid heating or cooling.

In this work, a novel, fast method for testing these repeated thermal stresses was used. A coated sample (30wt1000B05) was repeatedly heated in a self-built ultrafast furnace, displayed in **Figure 21** that was inspired by a setup developed by Wang et al.[54] It can be operated in an argon atmosphere by repeated evacuation and flooding of the chamber. A thin sample can be placed in between two carbon paper sheets that are resistively heated and the temperature is recorded by a pyrometer located above the middle of the sample. To determine the resistance of the coated sample to thermal cycling, it was rapidly heated and cooled by using the aforementioned novel ultrafast furnace. The rapid thermal cycling was performed for ten cycles.

In detail, a 30wt1000B05 sample was repeatedly heated for 20 s up to a temperature of 1260–1276 °C. The first cycle started at room temperature. After 2 s of heating, the temperature surpassed 700, 1200 °C was reached after 7 s and then the temperature plateaued at around 1260 °C. After that, the sample was allowed to cool down for 40 s, falling below the detection limit of the pyrometer of 700 °C after 4 s. This heating cycle was repeated a total of 10 times and the measured temperature is displayed in Figure 21.

Before the experiment starts, the naturally grown silicon oxide layer induces stress on the Si wafer, distorting the Si—Si bonds and creating an interface trap. Typically, if there are no phase transitions, during the heating, thermal stresses are reduced by the creep of the semi metallic substrate and eventually in the coating while in the cooling phase, compressive stresses develop within the layers due to the mismatch in the thermal expansion coefficient. In most cases, the repetition leads to the formation of microcracks to relax the thermomechanical stresses.[55,56] In this case however, the creep of the Si-substrate and coating are drastically reduced due to the short heating
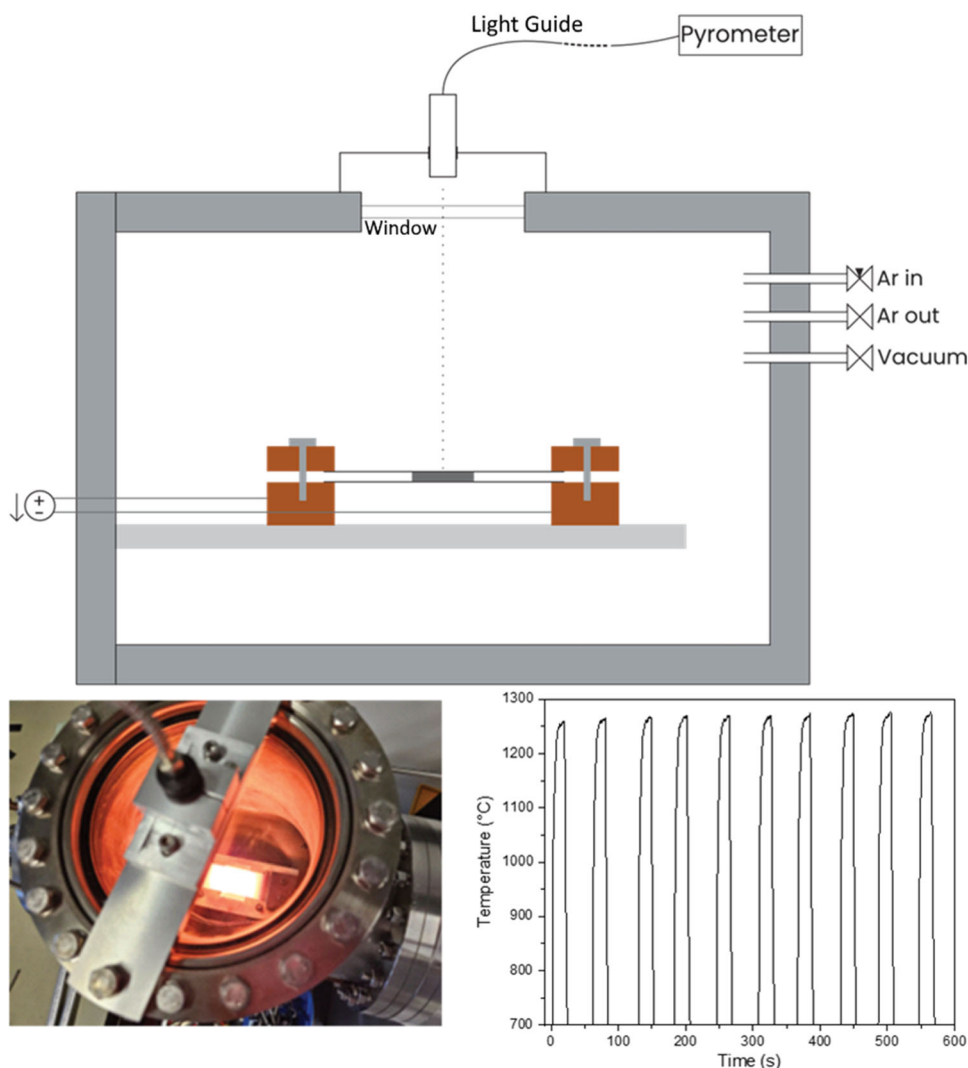
Figure 21. Sketch of the ultrafast furnace setup (top) with and image of the furnace in use (bottom left). Two carbon paper sheets are electrically heated by a controlled direct current. The temperature is measured by a pyrometer with a lower detection limit of 700 °C (temperature profile during rapid thermal cycling in bottom right).

times, thereby emphasizing significant stresses induced by phase changes and CTE mismatch. Still, the pyrolyzed 30 wt% B05 coating, after undergoing rapid thermal cycling, shows no damage, neither in light microscopy, electron microscopy nor in cross-section SEM images, as shown in **Figure 22** and **23**, respectively.

Even after extreme thermal conditions, the coating remains strongly adherent to the substrate, shows good quality, is even and homogeneous. It does not crack or spall off.

This excellent resistance against thermal shock is partly ascribed to the low CTE mismatch expected between substrate and coating. The CTE of silicon is $\approx 4.0 \times 10^{-6}\,\mathrm{K}^{-1}$ over the tested temperature range. The main phase of the coating is oxidized SiCN. SiCN has a CTE of ≈ 2.9–$3.5 \times 10^{-6}\,\mathrm{K}^{-1}$, amorphous SiOC without free carbon, which we expect to be relatively close in structure to the oxidized phase, has a CTE of $\approx 3.2 \times 10^{-6}\,\mathrm{K}^{-1}$ over the tested temperature range.[57]
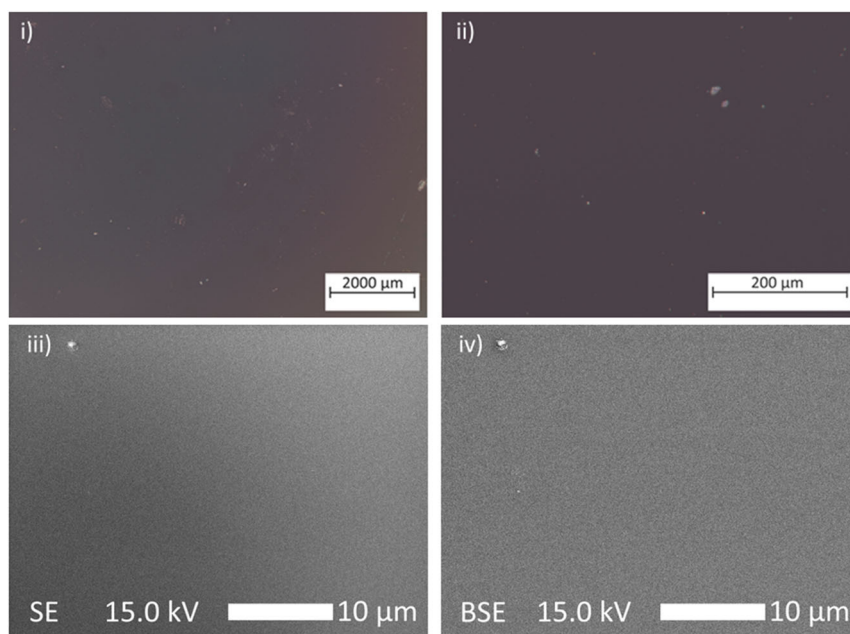
The introduced transition metals are expected to slightly increase the CTE of the ceramic film, further reducing this small difference, as their carbides HfC and TaC display CTEs of $\approx 6.2 \times 10^{-6}$ and $6.6 \times 0^{-6}\,\mathrm{K}^{-1}$,[58–61] and their oxides HfO_2 and Ta_2O_5 of $\approx 6.5 \times 10^{-6}$ and $3.5 \times 10^{-6}\,\mathrm{K}^{-1}$, respectively.[62,63]

Further contributors to the excellent thermal shock resistance are the homogeneity of the coating both in shape and element distribution, excellent adhesion and foremost to the absence of phase transformations due to the high crystallization resistance typical for PDCs.[21,22]

4. Conclusion

First investigations of $Si_x(Hf_{0.7}Ta_{0.3})_w(B_{var})C_yN_z$ polymers, obtained by chemical precursor modification of a commercial organopolysilazane Durazane 1800, show promising results

**ADVANCED
SCIENCE NEWS**

www.advancedsciencenews.com

**ADVANCED
ENGINEERING
MATERIALS**

www.aem-journal.com

Figure 22. Light microscopy images using a ring light source i) in low, ii) in high magnification and SEM images in iii) SE, and iv) BSE mode of 30wt1000B05 after repeated thermal shock.
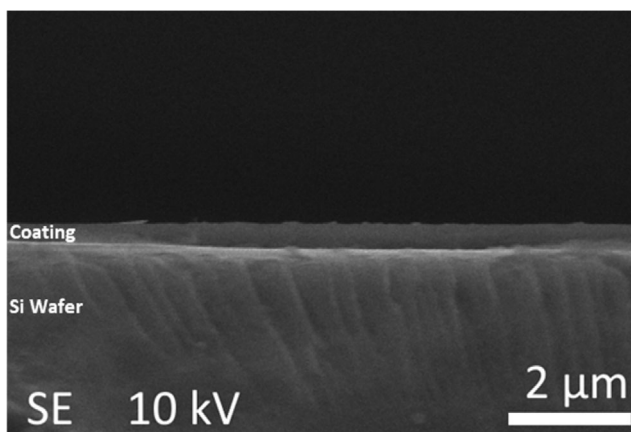
Figure 23. SEM image of the cross-section of 30wt1000B05 after repeated thermal shock.

for application as polymer-derived ceramic environmental barrier coatings by means of: 1) Good processability of the modified precursors as they remain viscous liquids that show good solubility in organic solvents with no low-mass molecules after vacuum drying, resulting in a low-mass loss of about 20% for powders and volume shrinkage of about 40% for coatings during pyrolysis in Ar at 1000 °C; 2) Precursor solutions of various concentrations yield homogeneous, even, and crack-free ceramic coatings of up to ≈540 nm thickness, showing good adhesion to the silicon substrate through facile spin-coating; and 3) A selected coating showed no damage after 10 h of oxidation at 1100 °C in air and excellent resistance to extreme temperature changes during repeated rapid thermal cycling.

Our findings reported here make coatings derived from $Si_x(Hf_{0.7}Ta_{0.3})_w(B_{var})C_yN_z$ precursors highly interesting for further investigations with respect to applications as advanced environmental or thermal barrier coatings where oxidation resistance, oxygen diffusivity, thermal conductivity, CTE, hardness, and application of thicker coatings on high-temperature substrate materials are of significant interest.

Supporting Information

Supporting Information is available from the Wiley Online Library or from the author.

Conflict of Interest

The authors declare no conflict of interest.

Data Availability Statement

The data that support the findings of this study are available from the corresponding author upon reasonable request.

[1] R. Darolia, *Int. Mater. Rev.* **2013**, *58*, 315.
[2] J. G. Thakare, C. Pandey, M. M. Mahapatra, R. S. Mulik, *Met. Mater. Int.* **2020**, *27*, 1947.
[3] D. Tejero-Martin, C. Bennet, T. Hussain, *J. Eur. Ceram. Soc.* **2021**, *41,*, 1747.
[4] S. T. Vagge, S. Ghogare, *Mater. Today: Proc.* **2022**, *56*, 1201.
[5] D. Ni, Y. Cheng, J. Zhang, J.-X. Liu, J. Zou, B. Chen, H. Wu, H. Li, S. Dong, J. Han, X. Zhang, Q. Fu, G.-J. Zhang, *J. Adv. Ceram.* **2022**, *11*, 1.
[6] W. G. Fahrenholtz, G. E. Hilmas, *Scr. Mater.* **2017**, *129*, 94.
[7] M. J. Gasch, D. T. Ellerby, S. M. Johnson, in *Handbook of Ceramic Composites* (Ed: N. P. Bansal), Kluwer, Boston, MA **2005**, pp. 197–224.
[8] L. Zoli, D. Sciti, A. Vinci, P. Galizia, F. Monteverde, S. Failla, L. Silvestroni, in *Encyclopedia of Materials: Technical Ceramics and Glasses*, (Ed: M. Pomeroy), Elsevier, Amsterdam, Netherlands **2021**, pp. 340–352.
[9] C. M. Carney, *J. Mater. Sci.* **2009**, *44*, 5673.
[10] E. Ionescu, S. Bernard, R. Lucas, P. Kroll, S. Ushakov, A. Navrotsky, R. Riedel, *Adv. Eng. Mater.* **2019**, *21*, 1900269.
[11] B. Feng, J. Peter, C. Fasel, Q. Wen, Y. Zhang, H.-J. Kleebe, E. Ionescu, *J. Am. Ceram. Soc.* **2020**, *103*, 7001.
[12] J. Yuan, S. Hapis, H. Breitzke, Y. Xu, C. Fasel, H.-J. Kleebe, G. Buntkowsky, R. Riedel, E. Ionescu, *Inorg. Chem.* **2014**, *53,*, 10443.
[13] A. S. Ulrich, T. Kaiser, E. Ionescu, R. Riedel, M. C. Galetz, *Oxid. Met.* **2019**, *92*, 281.
[14] Q. Wen, R. Riedel, E. Ionescu, *Adv. Eng. Mater.* **2019**, *21*, 1800879.
[15] Q. Wen, R. Riedel, E. Ionescu, *Corros. Sci.* **2018**, *145*, 191.
[16] J. Bai, K. Maute, S. R. Shah, R. Raj, *J. Am. Ceram. Soc.* **2007**, *90*, 170.
[17] Z. Gong, K. Guan, P. Rao, Q. Zeng, J. Liu, Z. Feng, *Front. Mater.* **2021**, *8*, 724377.
[18] X. Q. Cao, R. Vassen, D. Stoever, *J. Eur. Ceram. Soc.* **2004**, *24*, 1.
[19] K. N. Lee, *Surf. Coat. Technol.* **2000**, *133*, 1.
[20] P. Rohan, K. Neufuss, J. Matějíček, J. Dubský, L. Prchlík, C. Holzgartner, *Ceram. Int.* **2004**, *30*, 597.
[21] J. D. Torrey, R. K. Bordia, *J. Mater. Res.* **2007**, *22*, 1959.
[22] P. Colombo, G. Mera, R. Riedel, G. D. Sorarù, *J. Am. Ceram. Soc.* **2010**, *93*, 1805.
[23] A. Klausmann, K. Morita, K. E. Johanns, C. Fasel, K. Durst, G. Mera, R. Riedel, E. Ionescu, *J. Eur. Ceram. Soc.* **2015**, *35*, 3771.
[24] Y. Zhan, R. Grottenmüller, W. Li, F. Javaid, R. Riedel, *J. Appl. Polym. Sci.* **2021**, *138*, 50469.
[25] E. Ricohermoso III, F. Klug, H. Schlaak, R. Riedel, E. Ionescu, *Int. J. Appl. Ceram. Technol.* **2022**, *19*, 149.
[26] E. Ionescu, B. Papendorf, H.-J. Kleebe, H. Breitzke, K. Nonnenmacher, G. Buntkowsky, R. Riedel, *J. Eur. Ceram. Soc.* **2012**, *32*, 1873.
[27] J. Wang, V. Schölch, O. Görke, G. Schuck, X. Wang, G. Shao, S. Schorr, M. F. Bekheet, A. Gurlo, *Open Ceram.* **2020**, *1*, 100001.
[28] A. Viard, D. Fonblanc, M. Schmidt, A. Lale, C. Salameh, A. Soleilhavoup, M. Wynn, P. Champagne, S. Cerneaux, F. Babonneau, G. Chollon, F. Rossignol, C. Gervais, S. Bernard, *Chemistry* **2017**, *23*, 9076.

[29] H. Sheng, X. Huang, Z. Chen, Z. Zhao, H. Liu, *J. Phys. Chem. A* **2021**, *125*, 423.
[30] Q. Wen, Y. Xu, B. Xu, C. Fasel, O. Guillon, G. Buntkowsky, Z. Yu, R. Riedel, E. Ionescu, *Nanoscale* **2014**, *6*, 13678.
[31] P. Furtat, M. Lenz-Leite, E. Ionescu, R. A. F. Machado, G. Motz, *J. Mater. Chem. A* **2017**, *5*, 25509.
[32] Z. Yu, C. Zhou, R. Li, L. Yang, S. Li, H. Xia, *Ceram. Int.* **2012**, *38*, 4635.
[33] N. Brodie, J. P. Majoral, J. P. Disson, *Inorg. Chem.* **1993**, *32*, 4646.
[34] A. D. Bain, D. R. Eaton, A. E. Hamielec, M. Mlekuz, B. G. Sayer, *Macromolecules* **1989**, *22*, 3561.
[35] R. W. Dorn, E. A. Marro, M. P. Hanrahan, R. S. Klausen, A. J. Rossini, *Chem. Mater.* **2019**, *31*, 9168.
[36] I. Manners, *Synthetic Metal-Containing Polymers*, Wiley-VCH, Weinheim, Germany **2003**.
[37] M. Hellwig, A. Milanov, D. Barreca, J.-L. Deborde, R. Thomas, M. Winter, U. Kunze, R. A. Fischer, A. Devi, *Chem. Mater.* **2007**, *19*, 6077.
[38] X.-H. Zhang, S.-J. Chen, H. Cai, H.-J. Im, T. Chen, X. Yu, X. Chen, Z. Lin, Y.-D. Wu, Z.-L. Xue, *Organometallics* **2008**, *27*, 1338.
[39] D. Bahloul, M. Pereira, C. Gerardin, *J. Mater. Chem.* **1997**, *7*, 109.
[40] J. Seitz, J. Bill, N. Egger, F. Aldinger, *J. Eur. Ceram. Soc.* **1996**, *16*, 885.
[41] M. D. Fryzuk, J. Ballmann, R. F. Munhá, N. R. Halcovitch, in *Encyclopedia of Reagents for Organic Synthesis* (Eds: A. Charette, J. Bode, T. Rovis, R. Shenvi), John Wiley & Sons, Chichester, UK **2001**.
[42] A. Qazzazie-Hauser, K. Honnef, T. Hanemann, *Polymers* **2021**, *13*, 2424.
[43] P. Greil, *Adv. Eng. Mater.* **2000**, *2*, 339.
[44] D. Meyerhofer, *J. Appl. Phys.* **1978**, *49*, 3993.
[45] G. Barroso, Q. Li, R. K. Bordia, G. Motz, *J. Mater. Chem. A* **2019**, *7*, 1936.
[46] M. G. Clerici, F. Maspero, *Synthesis* **1980**, *1980*, 305.
[47] Q. Jiang, P. J. Carroll, D. H. Berry, *Organometallics* **1993**, *12*, 177.
[48] P. Colombo, T. E. Paulson, C. G. Pantano, *J. Sol-Gel Sci. Technol.* **1994**, *2*, 601.
[49] R. Williams, A. M. Goodman, *Appl. Phys. Lett.* **1974**, *25*, 531.
[50] G. Barroso, M. Döring, A. Horcher, A. Kienzle, G. Motz, *Adv. Mater. Interfaces* **2020**, *7*, 1901952.
[51] K. Wang, M. Günthner, G. Motz, B. D. Flinn, R. K. Bordia, *Langmuir* **2013**, *29*, 2889.
[52] C. Koch, T. J. Rinke, *Photolithography: Basics of Microstructuring*, MicroChemicals, Ulm, Germany **2017**.
[53] D. Amouzou, L. Fourdrinier, F. Maseri, R. Sporken, *Appl. Surf. Sci.* **2014**, *320*, 519.
[54] C. Wang, W. Ping, Q. Bai, H. Cui, R. Hensleigh, R. Wang, A. H. Brozena, Z. Xu, J. Dai, Y. Pei, C. Zheng, G. Pastel, J. Gao, X. Wang, H. Wang, J. Zhao, B. Yang, X. Zheng, J. Luo, Y. Mo, B. Dunn, L. Hu, *Science* **2020**, *368*, 521.
[55] V. Teixeira, M. Andritschky, W. Fischer, H. Buchkremer, D. Stöver, *J. Mater. Process. Technol.* **1999**, *92*, 209.
[56] A. C. Karaoglanli, K. Ogawa, A. Türk, I. Ozdemir, in *Progress in Gas Turbine Performance* (Ed: E. Benini), InTech, London, UK **2013**.
[57] C. Stabler, A. Reitz, P. Stein, B. Albert, R. Riedel, E. Ionescu, *Materials* **2018**, *11*, 279.
[58] Y. Okada, Y. Tokumaru, *J. Appl. Phys.* **1984**, *56*, 314.
[59] B. Santhosh, M. Biesuz, G. Domenico Sorarù, *Mater. Lett.* **2021**, *288*, 129336.
[60] Z. Zhang, Q. Li, S. C. Maiti, X. Shen, J. He, F. Peng, R. K. Bordia, *Int. J. Appl. Ceram. Technol.* **2023**, *20*, 1060.
[61] C. K. Jun, P. T. B. Shaffer, *J. Less Common Met.* **1971**, *24*, 323.
[62] B. Ohnysty, F. K. Rose, *J. Am. Ceram. Soc.* **1964**, *47*, 398.
[63] Y. S. Touloukian, R. K. Kirby, R. E. Taylor, T. Y. R. Lee, *Thermal Expansion, Nonmetallic Solids*, IFI/Plenum, New York, NY **1977**.